ce/papers
The online collection for conference papers in civil engineering
Ernst & Sohn A Wiley Brand

ORIGINAL ARTICLE

SDSS 2022
The International Colloquium on Stability and Ductility of Steel Structures
14-16 September, University of Aveiro, Portugal
Ernst & Sohn A Wiley Brand

Austenitic Stainless Steel EBF Subjected to Low and Extremely Low Cycle Fatigue

Lucy Lázaro[1], Rolando Chacón

Correspondence

Lucy Lázaro
Universitat Politècnica de Catalunya
Dep. Of Civil and Environmental Engineering
C/Jordi Girona 1-3
08034 Barcelona
lucy.laura.lazaro@upc.edu

Abstract

Dissipative zones buildings, in which plastic hinges or plastic strains occur during, for instance, seismic episodes, have been studied for many different types of steel fuse elements. Stainless steel (SS), has attracted attention in this regard due to its high ductility and further studies are needed to determine its performance and usefulness as fuses.

The use of SS in the construction industry has represented an advance due to its already known anticorrosive properties in addition to its strength and ductility. However, recent research on cyclic plasticity shows that SS has significant hardening properties, which can be exploited in the use of this material in structural elements to support cyclic loads, such as those occurring during earthquakes.

The cyclic plasticity models in SS have been studied with some applications (fatigue, low-cycle fatigue and extremely low cycle fatigue). Several studies carried out cyclic tests to obtain experimental data, which have been used for numerical models with the utilisation of a combined numerical model of kinematic/isotropic hardening. These studies recommend models to simulate the behaviour of SS under a cyclic load.

This work presents an experimental study of the cyclic behaviour of SS when subject to low and extremely low cycle fatigue. Several protocols on tests such as companion, multiple step and arbitrary tests were carried out. The results inferred from the experimental program provide hardening parameters used to study one example of dissipative zones of eccentrically braced frames (EBFs).

1 Introduction

Dissipative zones or fuse elements within a building are defined as the zones or elements that, when a low cyclic loading is presented, can dissipate energy through a bending, axial, or shear mechanism. When a cyclic event (seismic episode) occurs, the fuse elements need to achieve the plastic regime first, while the adjacent structural elements remain elastic. The design of fuse elements and its material need special attention when subject to low cyclic loading.

Stainless steel frames subjected to static loads have been under study in recent years [1-3] Recently, attempts for understanding SS fuse elements subjected to shear have been presented [4]. Results show enhanced ductility and strength with respect to other conventional carbon steels. Furthermore, tests of SS coupons subjected to low and extremely cyclic loading controlled by deformation show higher strain hardening than when subjected to monotonic test [5][6][7]. Consequently, the properties that can be exploited for the seismic design of buildings should take into account cyclic parameters from experimental data.

On the other hand, the application of SS in the seismic design of concentrically (CBFs) or eccentrically (EBFs) braced frames was studied [8]. The results revealed enhanced plastic deformations and excellent dissipation of energy. However, uncertainties related to the overstrength, a potentially undesired effect that affects the behaviour of the conceived plastic dissipation mechanism, have also been pointed out.

EBFs deserve careful consideration, because their configuration of columns, beams, and links (the fuse elements), might even allow the frames to be repaired via the replacement of links. It is worth mentioning that the mechanism of energy dissipation of a link is through shear strength in short links, and bending moment and shear strength in intermediate links. The link length is defined by its geometrical length and the ratio between its shear and moment plastic capacities.

[1] PhD Student, Universitat Politècnica de Catalunya

This study represents a calibrating example that is aimed at providing a basis for subsequent studies on EBFs of SS. Presently, these subsequent studies, under development by the authors, are related to the effect of the overstrength of SS links on the overall behaviour of EBFs.

2 Experimental data Stainless steel EN 1.4307 subjected to cyclic load

An experimental program was performed in 37 specimens of austenitic stainless steel EN 1.4307 subjected to cyclic load with several tests. The geometry of specimens is illustrated in figure 1:

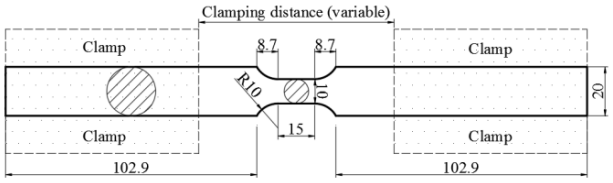

Figure 1: geometry of specimens (measures are in mm). Source: Reference [2]

The loading protocols are depicted in figure 2, where: figure 2a corresponds to companion test, 2b to multiple step test, and 2c to a tailor-made protocol of arbitrary variation of strain amplitudes. For the companion, strain cycles are identical. For the multiple step, strain increases systematically after ten cycles. For the tailor-made arbitrary protocol, strain amplitude varies according to a given time-series. Additionally, Fig. 2 (d) shows a novel type of test. Specimens are subjected to constant strain amplitude (10 cycles) in a first step. Subsequently, the same arbitrary strain amplitudes provided in (c) are used in this specimen "with a strain history".

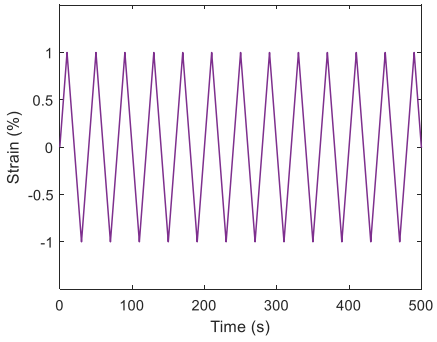

(a)

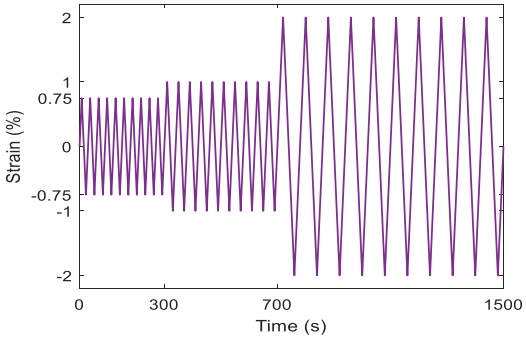

(b)

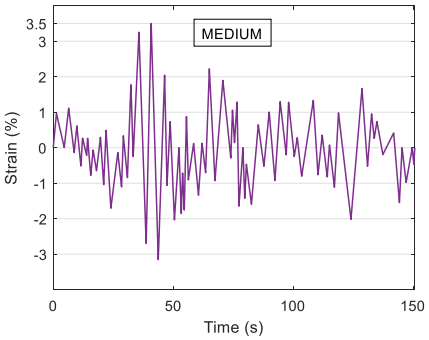

(c)

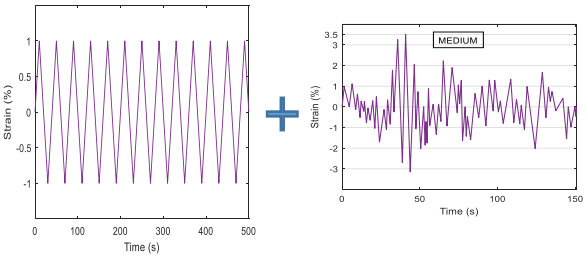

(d)

Figure 2: Load protocols for specimens. Source: Reference [2]

The results show high levels of strain hardening in SS, which confirms findings of previous studies [6][9]. The detail of the experimental program and main results are largely depicted in [5].

Several conundrums, such as the effect of the loading history as well as the effect of the level of strain on such history have been elucidated with these results. For instance, strain hardening was higher when the strain history had a strain amplitude of 2% (Figure 3a). It demonstrates the hardening of the material when it has a previous strain, whereas the hardening was lower when the strain history was 0.5% of strain amplitude. It indicates a little softening when SS is subjected to a smaller strain history (Figure 3b). Strain history may thus have both incremental and detrimental effects on the strain hardening.

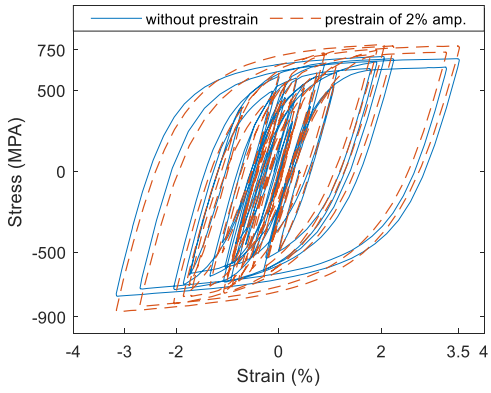

(a)

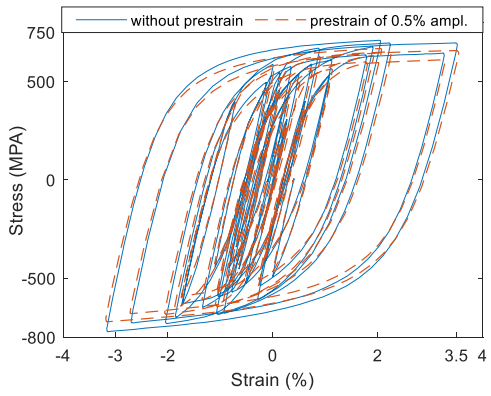

(b)

Figure 3: Tests results with and without prestrain.

3 Numerical study of eccentrically braced frame with stainless steel

A numerical study of EBFs with material results from experimental data was performed to evaluate the cyclic behaviour.

The EBFs studied have one bay and one storey with a horizontal link. The bay is 9m, the storey is 5.45m high for all models and the geometry and measures are depicted in figure 4. This frame is part of a building from [10] and has the same gravitational loads. Materials utilised were Austenitic Stainless Steel EN 1.4307 for links and Carbon Steel S355 (CS) for beams, columns and braces.

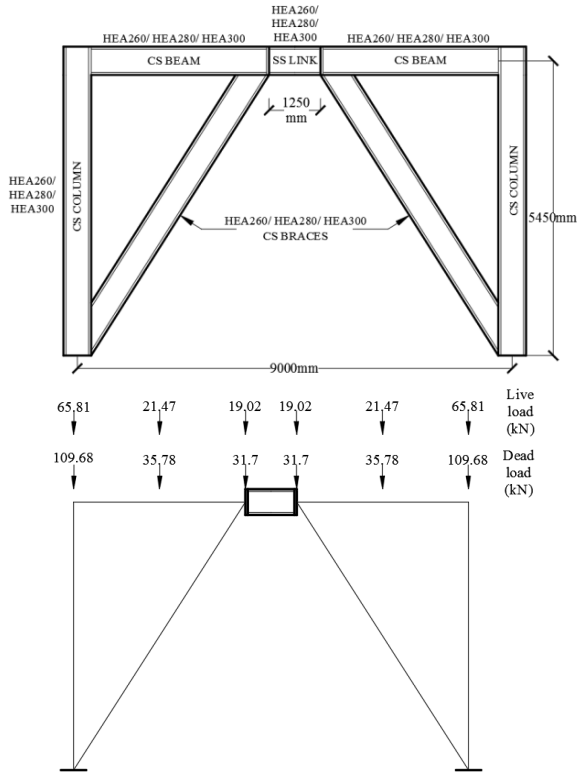

Figure 4: Geometry and gravitational load applied to frames. Source: Authors

A parametric study in with HEA260, HEA280, and HEA300 type cross-section links according to European standards was carried out. For all EBFs, the link length was 1250mm. This length allows to classify them into short links with $\rho<1.6$, where ρ is the nondimensional parameter link length or length ratio, which specifies the limits of the maximum design rotation [11].

In addition, a variation of thickness web (tw) of 6.5mm, 7.5mm, and 8mm was performed. Beams and braces possess the same link configuration without variation in their thickness web.

The Chaboche model [12] was used to implement the cyclic parameters within the numerical model.

4 Structural Analysis

Inelastic static and inelastic dynamic analyses were performed using Abaqus [13]. Beams, columns and braces were modelled as beam B31 type elements and links as shell S4R5 type elements. Ninety models were developed, 9 for inelastic static and 81 for inelastic dynamic analysis. The geometrical configuration ensured the strong column-weak beam mechanism.

4.1. Inelastic Static Analysis

This analysis was implemented through the application of a horizontal displacement located in a corner of the roof (figure 5). The displacement applied was 3% of the frame height, i.e. 160mm. The elastic and plastic properties of materials are specified in table 1. The cyclic properties of SS were selected from the experimental data and values are the average of strain amplitudes.

Table 1: Mechanics properties of materials. Source: Reference [5]

Material	Modulus of Elasticity E (N/mm^2)	Poisson U
CS S355	210000	0.3
AUST SS	184152.7	0.3

(a) Elastic properties

Material	Stress (N/mm^2)	Strain (mm/mm)
CS S355	0	0
	355	0.0017
	510	0.10831

(b) Plastic properties (Stress-strain pairs for CS)

Material	σ_o (N/mm^2)	Ck (N/mm^2)	γk	Q_∞	b
Austenitic SS	360	53611	185	111	1.56

(c) Parameters of combined isotropic/kinematic hardening model of cyclic plasticity (average values from [5])

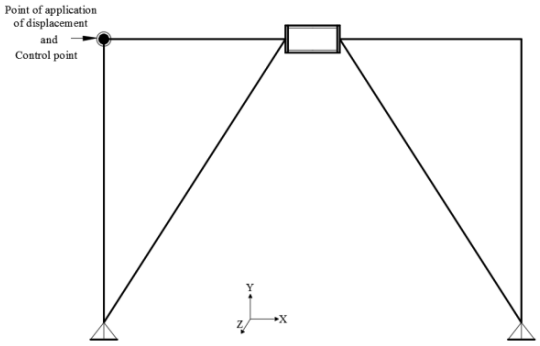

Figure 5: Location of applied displacement and control point. Source: Authors

The models were labelled according to the section type, thickness of the link and type of displacement applied. HEA260-M75 means EBF with HEA260 link, M for monotonic or static application and 75 for 7.5mm of link thickness.

4.2. Inelastic Dynamic Analysis

This analysis was implemented through a horizontal cyclic displacement of constant amplitude, which was placed in a corner of the roof (Figure 5). The constant amplitudes applied were 1%, 3% and 5% of the link strain after developing the inelastic static analysis. For obtaining such levels of strain, a previous monotonically incremental process showed roof displacements of 15.65mm, 37.14mm, and 55mm accordingly. The cyclic strain hardening parameters for SS, which correspond to 1%, 3%, and 5% [2] and their average, are established in table 2, whereas the properties of CS remain similar to inelastic analysis. Furthermore, we developed analyses based on the combined hardening model formulated in [12].

Table 2: Parameters of combined isotropic/kinematic hardening model of cyclic plasticity. Source: Reference [5]

Strain amplitude	σ_o (N/mm^2)	Ck (N/mm^2)	γk	Q_∞	b
1%	368	56622	307	101	0.28
3%	352	46645	191	127	1.94
5%	419	47692	131	149	131

(a) Specific values

Strain amplitude	Ck (N/mm^2)	γk	σ_o (N/mm^2)	Q_∞	b
0.75%	77270	70	360	111	1.56
1%	56622	307			
2%	59235	226			
2.5%	51750	215			
3%	46645	191			
3.5%	50175	181			
4%	39500	157			
5%	47692	131			

(b) Parameters for eight backstresses

Conundrums related to the most adequate selection of parameters for the inelastic analysis of a EBF arise. The choice of such parameters directly affect the results. Several comparisons between models are under development.

For instance, the comparison between models with a single cyclic hardening parameter (i.e., 1%), the average values of parameters obtained for all strain levels, and the application of eight backstresses for kinematic hardening parameters have been developed in a parametric study.

The models were labelled according to the section type, the thickness of the link, the type of loading, the strain amplitude applied, and the type of variation of cyclic hardening parameters utilised, which are A for average values, B for eight backstresses, and U for a single parameter. HEA260-D75-5A means EBF with HEA260 link, D for dynamic loading, 75 for 7.5mm of link thickness, 5 for 5% of strain amplitude, and A for the average of hardening parameters.

5 Discussion of results

5.1. Strength and deformation

The lateral resistance capacity of the EBFs is investigated through inelastic static analyses (monotonic). Figure 6 provides the displacement applied versus the basal shear for HEA260, HEA 280, and HEA300 with 75mm of the thickness of the link.

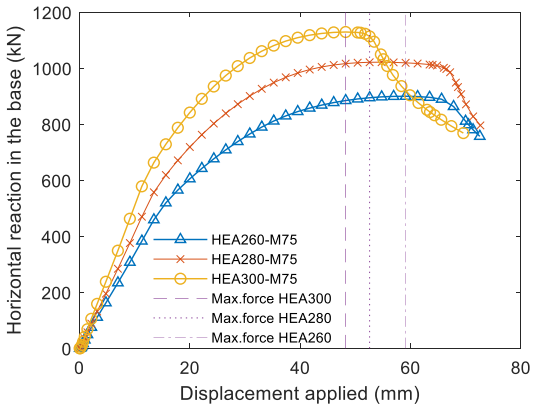

Figure 6: Displacement applied versus Horizontal reaction in the base.

In EBFs with bigger profile (HEA300), the maximum horizontal reaction in the base was higher, which was achieved at a lower displacement. On the other hand, in EBFs with smaller size (HEA260) the maximum horizontal reaction in the base was lower and achieved at a higher displacement, was lower (figure 6).

Another point of note was the decrease in the basal shear; HEA300 achieved its ultimate strength and posterior decrease in reaction early, while HEA280 and HEA260 reached them at a later stage.

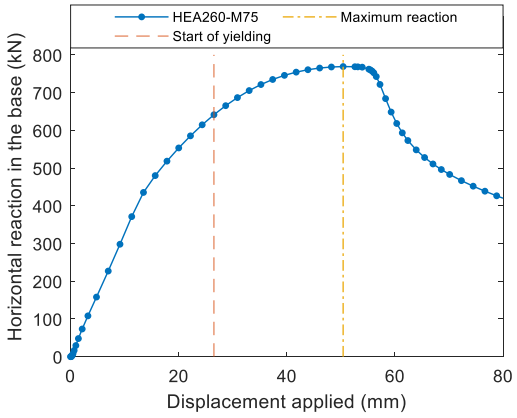

(a)

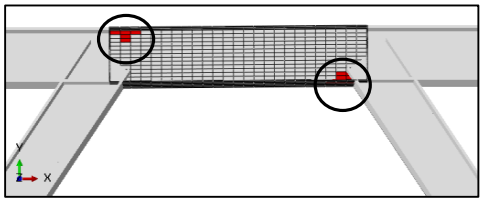

(b)

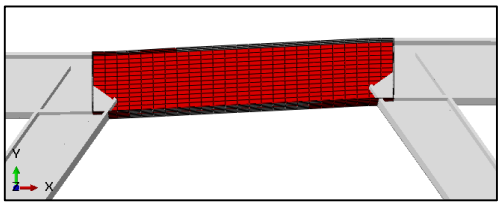

(c)

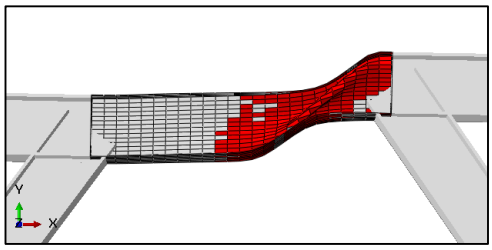

(d)

Figure 7: Link web after the yield strength.

Besides, in most models, the link web was the first to reach the yield strength. Figure 7a illustrates the horizontal reaction in the base versus the displacement applied curve of the model HEA260-M65. The corners of the link web (figure 7b) reached the yielding early, which indicates the initiation of shear deformation. When the horizontal reaction reached its maximum, the link web yielded completely (figure 7c). Beyond the peak reaction, the link failed through shear failure (figure 7d). The behaviour described above represents the desired behaviour of a EBF with dissipative zones.

5.2. In- and out-of-plane displacements at the web and the flanges

Figure 8a depicts the displacement in- and out-of-plane (U3) for EBFs with a HEA260 link with tw=6.5mm and ρ=1.44, which corresponds to a short link according to AISC [9] standards. Data were obtained from a node located in the link web with maximum variation of displacement.

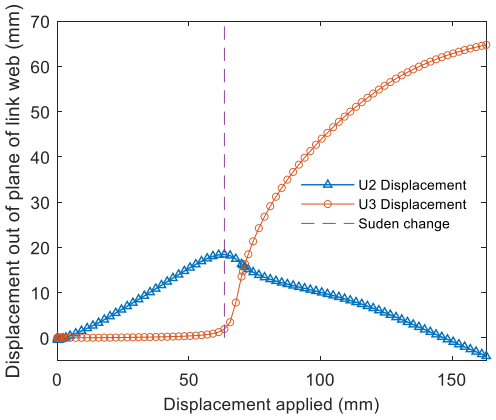

(a)

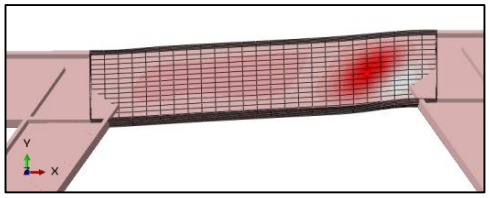

(b)

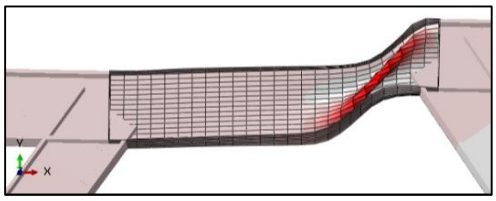

(c)

Figure 8: Displacement in a node of the link (model HEA260-M75).

A sudden change in out-of-plane displacement out was observed when the displacement applied was 63.45mm (figure 8a). This limit represents the initiation of the shear failure. Figure 8b shows the U3 displacement when the sudden change occurs, and figure 8c illustrates the maximum U3 displacement out of a plane.

The model in deformed configuration was taken to obtain the displacement of the link. Both ends of links presented maximum displacements in the vertical direction, which indicates a movement in opposite directions. This behaviour confirms the boundary conditions applied to study an isolated link [4][14].

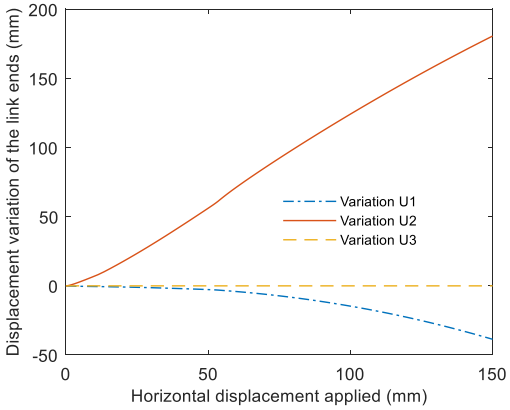

Figure 9: Displacement in ends of the link (model HEA300-M75).

For this reason, the strain was obtained from the variation of vertical displacement at the ends of the link. These values were taken to generate the cyclic displacement applied of 1%, 2%, and 3% of strain amplitude in the inelastic dynamic analysis.

5.3. Cyclic behaviour

The inelastic dynamic analyses to characterise the cyclic behaviour of the studied EBFs were accomplished. An appropriate application analysis of cyclic hardening parameters was realised.

For that purpose, additional results were presented by varying the following geometrical configurations: HEA280 on SS for links with tw=7.5mm, HEA280 on CS for beams and braces with tw=8mm, and HEA340 on CS for columns with tw=9.5mm. The labels of these EBFs are HEA280-D75-3A, HEA280-D75-3B, and HEA280-D75-3U. The displacement applied to these models was equivalent to 3% of strain of the link.

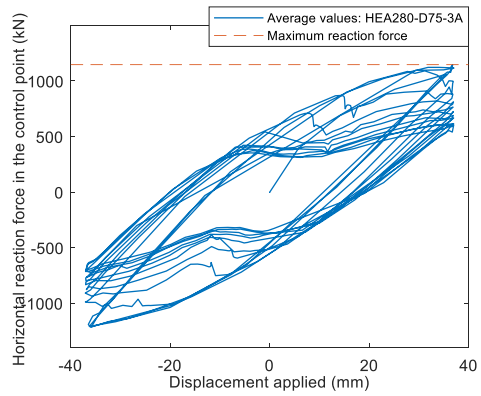

(a)

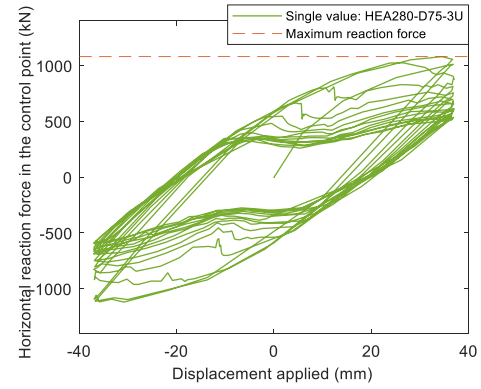

(b)

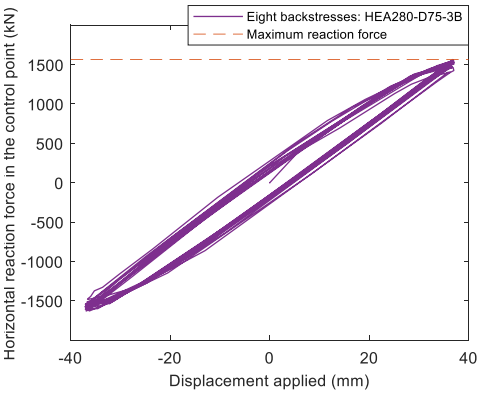

(c)

Figure 10: Comparison of hysteresis curves of HEA280-D75-3A, HEA280-D75-3B and HEA280-D75-3D models.

Figure 10 (a,b, and c) shows the hysteresis curves for three models with equal geometrical and material configurations. The unique difference was the form of application of cyclic hardening parameters.

Figure 10a exhibits the model with specific values of cyclic hardening parameters, i.e. material hardening parameters for 3% strain amplitude from experimental data (table 2a). Figure 10b shows the same model with the average values of hardening parameters (table 1c). Figure 10c illustrates the same model with one set of parameters for isotropic hardening and eight backstresses for kinematic hardening.

Hysteresis curves are fairly for assumptions a) and b). In contrast, the adoption of eight backstresses in kinematic hardening displays a significant variation in energy dissipated, and maximum reaction force reached.

Another point of view of the results shows the maximum horizontal reaction for each cycle. The values are similar to the first cycle for assumptions a) and b) as displayed in figure 11. Using specific values (HEA280-D75-3U), the maximum reaction decreased in the next cycles, whereas average values (HEA280-D75-3A) caused an increase in the maximum reaction in the next three cycles and a subsequent decrease. With eight backstresses (HEA280-D75-3B), the maximum reaction was higher and increased in the next cycles, where the hardening can be seen.

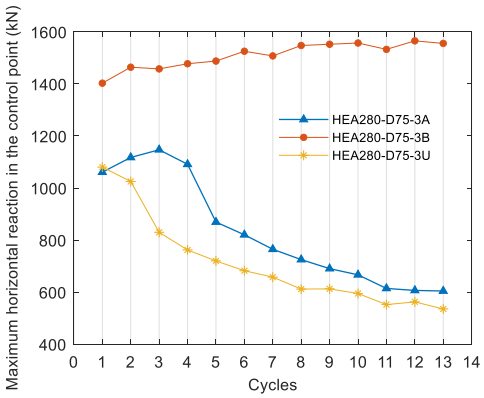

Figure 11: Maximum horizontal reaction force in the control point for each cycle.

Curves from figure 11 demonstrate a certain similitude between HEA280-D75-3U and HEA280-D75-3A models and a significant variation for HEA280-D75-3B. Consequently, it is necessary to emphasise the selection and application of cyclic hardening parameters.

Additionally, the variation of strain amplitudes applied was analysed. For 1% of strain amplitude, all EBFs presented a behaviour close to elastic range, i.e. with a little energy dissipated. In all models with this strain amplitude, no elements reached the yield strength. For 3% of strain amplitude, in most cases, the EBFs developed approximately three cycles and next the links achieved the yield strength with the consequent shear failure of the structure. For 5% of strain amplitude applied, the EBFs only completed one cycle or less in all models and the structure immediately exhibited the shear failure.

Figure 12 displays the displacement applied versus the horizontal reaction in the control point curves for 1% (figure 12a) , 3% (figure 12b), and 5% (figure 12c) of strain amplitudes.

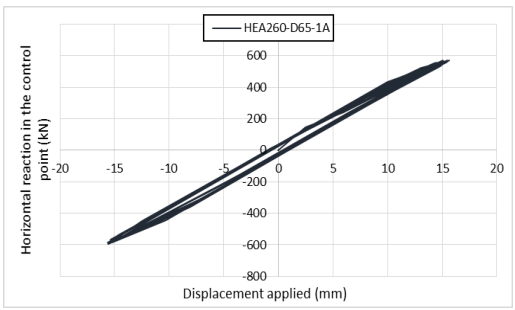

(a)

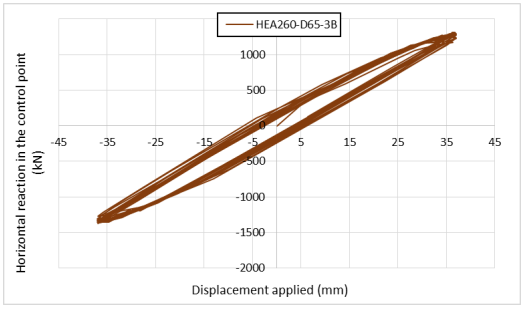

(b)

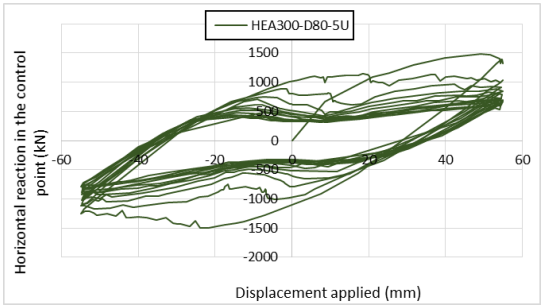

(c)

Figure 12: Hysteresis curves for 1%, 3%, and 5% of strain amplitude applied.

A particular issue was revealed in EBFs with the geometrical configuration of HEA260 on SS for links with tw=7.5mm, HEA260 on CS for beams and braces with tw=8mm, and HEA340 on CS for columns with tw=9.5mm. Note that t_w of the link is lower than t_w of the beams, and the link should achieve the plastic regimen first. However, the beams produce the yield strength in parallel with the link.

The hatched area in figure 13a shows the yield strength. The link achieves the yield strength completely and the joint of the beam with the link reaches it at the same instant.

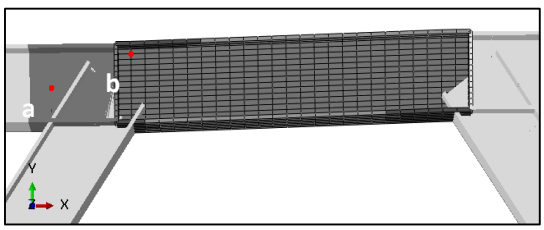

(a)

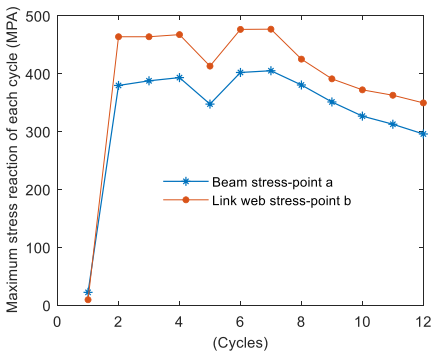

(b)

Figure 13: Maximum stresses in the beam and the link web of HEA260-D75-3A model.

Maximum principal stresses of each cycle were drawn (figure 13b) for points "a" and "b". Point "a" is located in the beam and point "b" in the link (figure 13a), which reached the yield strength early. Maximum stresses in the beam were lower than those developed by the link.

This behaviour exhibits the cyclic hardening properties of SS. The link with SS and the beam with CS moved simultaneously to the inelastic stage, which represents an undesirable behaviour of the EBF. Therefore, extensive research concerning the overstrength of SS is required.

6 Conclusions

The target of this study was the understanding the cyclic behaviour and low cycle fatigue of austenitic stainless steel EN 1.4307 for seismic use purposes when intended for dissipative zones in EBFs. The conclusions of this study are as follows.

An experimental program was performed on 37 specimens subjected to several strain protocol tests and was observed that the strain history or preload influences directly the hardening of the material.

A parametric numerical study for a calibrating model was developed. A hybrid EBFs with CS for beams, columns and braces, and SS for links was carried out. In the inelastic static analysis, EBFs achieved the desired behaviour, whereas, in inelastic dynamic, a particular issue was observed, the beam and the link moved to the inelastic stage simultaneously. Therefore, further research concerning the overstrength of SS is required

The dynamic analyses also showed that the way to use of the cyclic hardening parameters influences the cyclic behaviour of EBFs . This study used the average values of the cyclic hardening parameters.

7 Acknowledgments

The authors acknowledge the financial support provided by the Project BIA2016-75678-R, AEI/FEDER, UE "Comportamiento estructural de pórticos de acero inoxidable. Seguridad frente a acciones accidentales de sismo y fuego", funded by the Spanish Ministry of Economic Affairs and Digital Transformation (MINECO). The first author acknowledges the financial support from the Peruvian Government. Beca Generación del Bicentenario.

References

[1] Y. Shen and R. Chacón. "Geometrically non-linear analysis with stiffness reduction for the stability design of stainless steel structures: Application to members and planar frames," *Thin-Walled Structures*, vol. 148, 160581, 2020.

[2] I. Arrayago, I. González-de-León, E. Real, E. Mirambell, "Tests on stainless steel frames. Part I: Preliminary tests and experimental set-up," *Thin-Walled Structures*, vol. 157, 107005, 2020.

[3] F. Walport, M. Kukucler and L. Gardner, "Stability Design of Stainless Steel Structures" *J. Structural Engineering*, vol. 148 (1), 2022.

[4] R. Chacón, A. Vega, and E. Mirambell, "Numerical study on stainless steel I-shaped links on eccentrically braced frames," *J. Constr. Steel Res.*, vol. 159, pp. 67–80, 2019.

[5] L. Lazaro and R. Chacón, "Material behaviour of austenitic stainless steel subjected to cyclic and arbitrary loading," vol. 189, 2022.

[6] S. Zheng, F. Zhou, J. Cheng, H. Li, and R. Rong, "Experimental study on cyclic hardening characteristics of structural stainless steels," *J. Constr. Steel Res.*, vol. 191, no. January, p. 107196, 2022.

[7] K. H. Nip, L. Gardner, C. M. Davies, and A. Y. Elghazouli, "Extremely low cycle fatigue tests on structural carbon steel and stainless steel," *J. Constr. Steel Res.*, vol. 66, no. 1, pp. 96–110, 2010.

[8] L. DiSarno, A. S. Elnashai, and D. A. Nethercot, "Seismic response of stainless steel braced frames," *J. Constr. Steel Res.*, vol. 64, no. 7–8, pp. 914–925, 2008.

[9] S. H. Heng *et al.*, "Effect of loading protocol on the mechanical properties of 316L stainless steel Effect of loading protocol on the mechanical properties of 316L stainless steel," *J. Phys. Conf. Ser.*, 2021.

[10] M. Bruneau, C.-M. Uang, and R. Sabelli, *Ductile Desing of Steel Structures*. Second Edition 2011.

[11] A. 345-05, "AISC Seismic Provisions for Structural Steel Buildings." American Institute of Steel Construction, Chicago (IL).

[12] J. L. Chaboche, "A review of some plasticity and viscoplasticity constitutive theories," *Int. J. Plast.*, vol. 24, no. 10, pp. 1642–1693, 2008.

[13] Abaqus. Simulia Dassault Systèmes, 2021.

[14] P. W. Richards and C.-M. Uang, "Effect of Flange Width-Thickness Ratio on Eccentrically Braced Frames Link Cyclic Rotation Capacity," *J. Struct. Eng.*, vol. 131, no. 10, pp. 1546–1552, 2005.